Optik 127 (2016) 985–990

Contents lists available at ScienceDirect

Optik

journal homepage: www.elsevier.de/ijleo

A new hybrid algorithm for co-phasing segmented active optical system based on phase diversity

D. Yue [a,b], S.Y. Xu [a,*], H.T. Nie [a,b], B.Q. Xu [a], Z.Y. Wang [a]

[a] Department of Space Optics, Changchun Institute of Optics, Fine Mechanics and Physics, Chinese Academy of Sciences, Changchun 130033, China
[b] University of the Chinese Academy of Sciences, Beijing 100039, China

ARTICLE INFO

Article history:
Received 9 February 2015
Accepted 29 October 2015

Keywords:
Segmented mirror
Co-phasing error
Phase diversity
Adaptive genetic algorithm
Linear correction algorithm

ABSTRACT

In order to reach its diffraction limited performance, the co-phase errors of segmented mirror synthetic aperture optics (SAO) systems must be accurately measured and corrected. A new hybrid algorithm based on phase diversity is proposed for co-phasing the segmented mirrors. It utilizes an improved adaptive genetic algorithm to determine the global initial aberration coefficients, and then uses an iterative linear correction algorithm to obtain the linear estimator of coefficients under small residual phase after initial alignment of the system. The numerical simulation results demonstrate that the proposed method is highly sensitive and noise tolerant. It can fulfill the requirements for the phasing of segmented mirror telescopes and retrieving the unknown object for the system.

1. Introduction

Segmented mirror synthetic aperture optics (SAO) systems can meet the demands of the next generation space telescopes being lighter, larger and foldable [1]. Segmented primary mirror stitches serials of sub-mirrors together to reach the optimal capabilities of a monolithic one. This kind of space telescopes can be folded for launch and deploy autonomously after reaching orbit. However, only if co-phasing of the segmented mirrors is achieved, can it provide a high quality image equivalent to that of a monolithic mirror. Co-phasing a segmented mirror is to remove the misalignments, including relative piston aberrations between segments and tip/tilt aberrations of each segment.

Many methods are proposed for co-phasing the segmented mirror to obtain nearly diffraction limited performance from the total aperture, such as curvature sensing [2], modified Hartmann–Shack wavefront sensing (WFS) [3], phase retrieval based on PSF data sets [4], modified peak ratio technique [5], Michelson interferometry [6] and phase diversity WFS [7–10] etc. PD WFS outstands in the development of segmented active optical systems where traditional wavefront reconstruction like using Shack–Hartmann wavefront sensing tends to break down at the mirror segment edges. Additionally, this approach requires no new instrumentation be added to the already complicated optical system and is considerably sensitive to both relative piston and tip/tilt aberrations for continuous and discontinuous input distorted wavefront.

This paper presents a new hybrid algorithm based on phase diversity aimed at massive sub-apertures of segmented primary mirror. The number of variables needing to be solved from the non-linear optimization problem increases triply as that of sub-mirrors, which slows down the convergence speed significantly. Since genetic algorithm (GA) [11–13] is a global probability search method, by taking advantage of which global initial value of Zernike aberration coefficients can be obtained. After initial alignment by active segmented primary mirror analog system, linearization the expression of the OTFs in each diversity plane can be processed under the small residual aberrations. This hybrid algorithm can avoid converging to local optima, reduce the computational complexity, improve the convergence speed and provide higher calculation accuracy.

2. Basic theory

2.1. Theoretical analysis of co-phase errors impact on segmented space telescope

The generalized pupil function of the segmented primary mirror is given by Eq. (1):

$$P(\varepsilon,\eta)=\sum_{n=1}^{N}P_n(\varepsilon,\eta)=\sum_{n=1}^{N}p_n(\varepsilon,\eta)\ \exp\left[i\varphi_n(\varepsilon,\eta)\right] \tag{1}$$

* Corresponding author. Tel.: +86 15843149856.
E-mail address: danzik3@126.com (S.Y. Xu).

http://dx.doi.org/10.1016/j.ijleo.2015.10.218
0030-4026/

where, (ε, η) is the coordinate of pupil plane, n is the index of sub-aperture. P_n donates complex pupil function of nth segmented sub-mirror, p_n and φ_n are its amplitude and phase separately. The shape function of sub-aperture in the pupil plane p_n is given by formula (2):

$$p_n(\varepsilon, \eta) = \begin{cases} 1 & \text{inside the sub-aperture} \\ 0 & \text{outside the sub-aperture} \end{cases} \tag{2}$$

In case to simply the situation, just like Keck [14], all the sub-apertures are assumed to have the same shape and are perfect without high-order aberrations except co-phasing errors, namely pistons and tip–tilts. Thus the generalized pupil can be rewritten as function (3):

$$P(\varepsilon, \eta) = \sum_{n=1}^{N} p_n(\varepsilon, \eta) \exp\left[i\frac{2\pi}{\lambda}(e_n + T_{xn} + T_{yn})\right] \tag{3}$$

where, e_n and T_{xn}, T_{yn} represent piston and tip–tilts errors respectively.

Using the principles of Fourier optics, corresponding incoherent point spread function (PSF) of the image plane $s(u, v)$ can be gained by Eq. (4):

$$\begin{aligned} s(u, v) &= \left|h(u, v)\right|^2 \\ &= \left|\Im\left\{\sum_{n=1}^{N} p_n(\varepsilon, \eta) \exp\left[i\frac{2\pi}{\lambda}(e_n + T_{xn} + T_{yn})\right]\right\}\right|^2 \end{aligned} \tag{4}$$

where, (u, v) are position vector in the image plane, $h(u, v)$ donates coherent impulse response function and $\Im\{\}$ is the Fourier transform operator. According to paper [15], $h(u, v)$ is given by formula (5):

$$\begin{aligned} &h(u, v) \\ &= \sum_{n=1}^{N} [\Im\{\exp[jkf_n(\varepsilon, \eta)]\} * \Pi(u, v)] \\ &\times \exp[jk(\alpha_n - \lambda u\varepsilon_n - \lambda v\eta_n) \end{aligned} \tag{5}$$

among which, $\Pi(u, v)$ is Fourier transform of sub-aperture's pupil function, wave number is $k = 2\pi/\lambda$, α_n and $f_n(\varepsilon, \eta)$ denotes the pistons and the remaining tip–tilts aberration of the nth sub-aperture respectively.

Above equations reveal relevant physical significance, coupled with the relative offsets of pupil centers in different sub-apertures, co-phase errors affect the far-field image of system directly and $\Pi(u, v)$ reflects the impact of sub-aperture pupil.

Thus it can be seen that, in segmented extremely large telescope, how to co-phase its segmented primary mirror to achieve the ultimate resolution is an unavoidable problem. The key issue to solve the problem depends on whether the pistons among the segments and their tip–tilts can be measured and corrected with very high accuracy.

2.2. Theoretical derivation of PD cost function

The PD reconstructed algorithm not only can be used to detect the continuous wavefront aberration caused by atmospheric turbulence or surface error of optical elements, but also is very sensitive to the discontinuous aberrations such as relative piston errors between segments and tip/tilt aberrations of each segment. The major issue is to detect the phase distortion or aberration coefficients in an incoming wavefront by one image recorded in the focal plane and the other one recorded in an out-of-focus plane of the optical system simultaneously under circumstance that both object distribution and optical transfer function of atmosphere-telescope synthetic system are unknown.

Based on least-square approach, a cost function is presented by Eq. (6) in frequency domain to fit the data such that the total RMS difference between the images observed in the different channels and those assumed by the imaging mode:

$$L[I_k; o, \{e_j, T_{xj}, T_{yj}\}] = \sum_{k=1}^{K}\sum_{f_u, f_v}[I_k(f_u, f_v) - O(f_u, f_v)S_k(f_u, f_v)]^2 \tag{6}$$

where, (f_u, f_v) is the coordinate in frequency domain, I_k and O represent the Fourier transforms of the kth image intensity and object distribution respectively, S_k is the optical transfer function (OTF) of the kth image plane and K is the total images number.

In order to eliminate the dependence of the cost function L on object frequency spectrum O in the optimization process, the partial differential of L with respect to O is set to equal zero, then the following formula (7) can be obtained:

$$O = \frac{\sum_{k=1}^{K} I_k S_k^*}{\sum_{k=1}^{K}\left|S_k\right|^2 + \gamma} \tag{7}$$

Thus the cost function L is solved for simplification as Eq. (8):

$$L = \sum_{f \in \chi}\sum_{k}\left|I_k\right|^2 - \sum_{f \in \chi}\frac{\left|\sum_k I_k S_k^*\right|^2}{\sum_k\left|S_k\right|^2 + \gamma} \tag{8}$$

among which, γ is the regularized coefficient which guarantees the existence and uniqueness of solutions. Then the problem of estimating phase distribution or aberration coefficients of the wavefront is transferred to optimize the functional L, namely to find the coefficient set for which the cost function [Eq. (8)], is a minimum.

2.3. Search algorithms to optimize the PD cost function

Many search algorithms have been proposed to optimize the PD cost function, such as conjugate gradient method, quasi-Newton method, neural network algorithm and genetic algorithm. The gradient of cost function needs to be deduced while using conjugate gradient method or quasi-Newton algorithm, which adds the calculation complexity and is prone to converge to local optima. Neural network optimization algorithm has to process highly cumbersome network training to massive images. Genetic algorithm (GA) is a global probability search method, it only needs the information of cost function and do not need to deduce its gradient, which simplify the calculation procedure and has a better global convergence. However, GA is also very complex and has a quite limited usage in real-time correction algorithms.

Thus this paper presents a new hybrid algorithm, which uses improved adaptive GA to obtain the global initial coefficients of distorted phase by utilizing smaller population size and fewer evolution generations and then linearizes OTF under small residual phase aberrations to decrease the calculation complex and increase the convergence speed.

2.3.1. Improved adaptive GA

The flow chart of improved adaptive GA based on PD is shown in Fig. 1.

For special note, the increase in number of sub-mirrors will lead to massive variables needed to be optimized. Therefore multi-point crossover and mutation are applied to accelerate the convergence rate. Meanwhile, due to priori knowledge, when piston errors between segments approach $\lambda/2$, it is prone to fall into local extreme around the negative value of piston errors. In order to solve this problem, piston errors of the best individual among each new

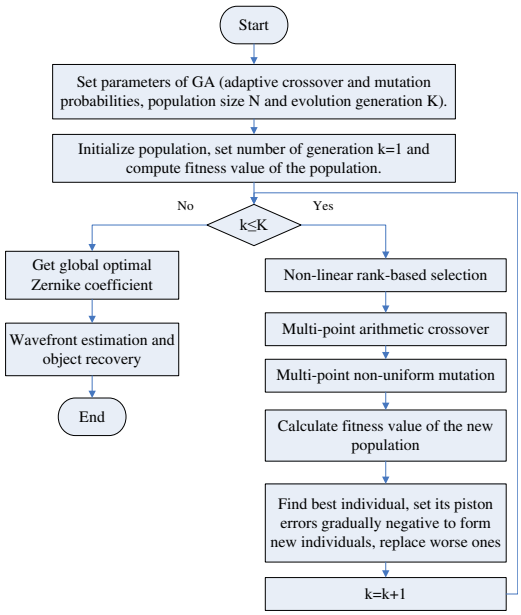

Fig. 1. Flow chart of PD based improved adaptive GA.

population are set to their negative values gradually to form new individuals, which are used to substitute for the worse ones. Among the new individuals, there must be one close to the global extreme.

2.3.2. Linear correction algorithm based on PD

Due to the high calculation complexity, nonlinear PD has a limited usage in real-time correction algorithms [16]. Through linearization of OTF to recovery wavefront under small residual phase [17], it can simplify the calculation procedure and provide more accurate results.

First, linearize the expression of the OTFs in each diversity plane by first-order Taylor expansion as Eq. (9):

$$S_k = S_k(\boldsymbol{\alpha}_0) + \nabla S_k(\boldsymbol{\alpha}_0)\cdot\boldsymbol{\alpha} + o\|\boldsymbol{\alpha}\|^2 \quad (k=1,2) \tag{9}$$

where, $\boldsymbol{\alpha}$ is a row vector of sub-mirrors' Zernike coefficients, $S_k(\boldsymbol{\alpha}_0)$ is OTFs value at coefficient vector $\boldsymbol{\alpha}_0$, $\nabla S_k(\boldsymbol{\alpha}_0)$ is the first-order differentiation value at $\boldsymbol{\alpha}_0$ for each of these OTFs, $o\|\boldsymbol{\alpha}\|^2$ donates the high order remainder. $k=1,2$ represent OTFs in the focal plane and out-of-focus plane respectively.

Taking Eq. (9) into formula (8), then the cost function can be rewritten as expression (10):

$$\begin{aligned} L &= \sum_f \left[\sum_{k=1}^{2} \left|I_k\right|^2 - \frac{\left|\sum_{k=1}^{2} I_k\cdot S_k^*(\boldsymbol{\alpha}_0) + \sum_{k=1}^{2} I_k\cdot(\nabla S_k(\boldsymbol{\alpha}_0)\boldsymbol{\alpha})^*\right|^2}{\sum_{k=1}^{2}\left|S_k(\boldsymbol{\alpha}_0)\right|^2+\gamma} \right] \\ &= \sum_f \left[\sum_{k=1}^{2} \left|I_k\right|^2 - \left|\mathbf{A}\boldsymbol{\alpha}+B\right|^2 \right] \end{aligned} \tag{10}$$

where:

$$\begin{aligned} \mathbf{A}(f) &= \frac{I_1\cdot\nabla\mathbf{S}_1^*(\boldsymbol{\alpha}_0) + I_2\cdot\nabla\mathbf{S}_2^*(\boldsymbol{\alpha}_0)}{\sqrt{\left|S_1(\boldsymbol{\alpha}_0)\right|^2+\left|S_2(\boldsymbol{\alpha}_0)\right|^2+\gamma}} \\ B(f) &= \frac{I_1\cdot\mathbf{S}_1^*(\boldsymbol{\alpha}_0) + I_2\cdot\mathbf{S}_2^*(\boldsymbol{\alpha}_0)}{\sqrt{\left|S_1(\boldsymbol{\alpha}_0)\right|^2+\left|S_2(\boldsymbol{\alpha}_0)\right|^2+\gamma}} \end{aligned} \tag{11}$$

In order to minimize the cost function, its first derivative is derived with respect to aberration coefficients as Eq. (12):

$$\frac{\partial L}{\partial\boldsymbol{\alpha}} = -\frac{\partial}{\partial\boldsymbol{\alpha}}\sum_f\left|\mathbf{A}\boldsymbol{\alpha}+B\right|^2 = -2\,\mathrm{Re}\left\{\sum_f[(\mathbf{A}\boldsymbol{\alpha}+B)^*\cdot\mathbf{A}]\right\} \tag{12}$$

Set $\partial L/\partial\boldsymbol{\alpha}=0$, thus the linear estimation of $\boldsymbol{\alpha}$ can be given by Eq. (13):

$$\hat{\boldsymbol{\alpha}} = \left[Re\left(\sum_f \mathbf{A}^*\mathbf{A}\right)\right]^{\dagger}\mathrm{Re}\left[\sum_f(-B^*\mathbf{A})\right] \tag{13}$$

where, Re means the real part of matrix and † donates the generalized inverse of a matrix.

For deducing the gradient of OTF with respect to co-phase errors, the aberration coefficient of mth sub-mirror is defined as three-dimensional vector by Eq. (14):

$$\boldsymbol{\alpha}_m = (e_m, tx_m, ty_m) \tag{14}$$

Thus, partial derivative of OTF to unknown co-phase errors $\boldsymbol{\alpha}$ is given by expression (15):

$$\nabla S_k(\boldsymbol{\alpha}) = \begin{bmatrix} \partial S_k/\partial\boldsymbol{\alpha}_1 \\ \vdots \\ \partial S_k/\partial\boldsymbol{\alpha}_m \\ \vdots \\ \partial S_k/\partial\boldsymbol{\alpha}_N \end{bmatrix} \tag{15}$$

where:

$$\frac{\partial S_k}{\partial\boldsymbol{\alpha}_m} = \left(\frac{\partial S_k}{\partial e_m}, \frac{\partial S_k}{\partial tx_m}, \frac{\partial S_k}{\partial ty_m}\right) \tag{16}$$

Assuming the phase of mth sub-mirror is as Eq. (17):

$$\varphi_m = 2\pi(e_m Z_{0m} + tx_m Z_{1m} + ty_m Z_{2m}) \tag{17}$$

with Z_{0m}, Z_{1m} and Z_{2m} are the first three order Zernike circular polynomials, then the first order derivative of OTF with respect to piston and tip/tilt errors are given by Eq. (18):

$$\begin{aligned} \frac{\partial S_k}{\partial e_m} &= \Im\{2\ \mathrm{Re}\,[\Im\{i2\pi Z_{0m}p_m\ \exp(i\varphi_m)\exp(i\varphi_{dk})\}\cdot h_k^*]\} \\ \frac{\partial S_k}{\partial tx_m} &= \Im\{2\ \mathrm{Re}\,[\Im\{i2\pi Z_{1m}p_m\ \exp(i\varphi_m)\exp(i\varphi_{dk})\}\cdot h_k^*]\} \\ \frac{\partial S_k}{\partial ty_m} &= \Im\{2\ \mathrm{Re}\,[\Im\{i2\pi Z_{2m}p_m\ \exp(i\varphi_m)\exp(i\varphi_{dk})\}\cdot h_k^*]\} \end{aligned} \tag{18}$$

where, φ_{dk} is the known defocused aberration introduced by the kth defocused amount, which is defined as Eq. (19):

$$\varphi_{dk}^{PV} = \begin{cases} 0 & k=1 \\ \dfrac{d}{8\lambda(F^{\#})^2} & k=2 \end{cases} \tag{19}$$

3. Numerical simulation

In this section, numerical simulations are processed to measure the co-phase errors of the segmented primary mirror and recovery the far-field object by utilizing the proposed algorithms in Section 2 under the incoherent illumination.

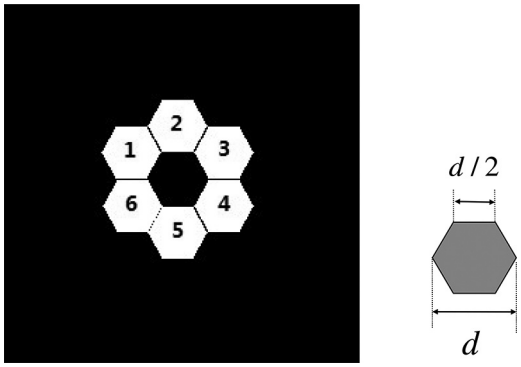

Fig. 2. Construction of primary mirror and segment sub-aperture's dimensions.

Table 1
A set of random co-phase errors for simulation.

Index of sub-mirrors	Piston/λ	Tilt/λ	Tip/λ
1	0	0	0
2	−0.4	0.25	−0.3
3	0	−0.38	0.4
4	0.35	0.4	−0.3
5	0.18	0	−0.26
6	0.3	0	0

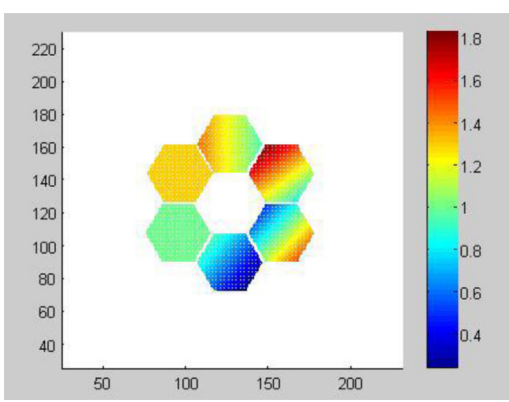

Fig. 3. Wavefront co-phase errors distribution.

3.1. Utilize improved adaptive GA to confirm the global initial coefficients

The parameters of the optical system used in the simulation are as following. The segmented primary mirror consists of 6 hexagon sub-mirrors; their construction and sequence are shown in Fig. 2:

The hexagon sub-mirror's diameter is d and occupies 43×43 pixels of the pupil plane. The diameter of the primary mirror is D and its corresponding pixels are 128×128. In order to satisfy the Nyquist sample theory, the whole pupil plane is set to 256×256 pixels. The $F^{\#}$ of optical system is 8, monochromatic wavelength is 570 nm and the defocused distance is set to 400λ.

Set *1*st sub-mirror a standard mirror, a set of random piston and tip/tilt errors listed in Table 1 are applied to all sub-apertures:

Then the distribution of distorted wavefront co-phase is shown in Fig. 3:

Using a satellite picture of an urban scene as object, diffraction limited image of the segmented optical imaging system can be simulated when all sub-apertures are in ideal position. Fig. 4 shows the corresponding images:

Assuming the intensity distribution of the CCD camera's readout noise approximates Gaussian noise model, a pair of focal and defocused images with noise collected by CCD camera are shown as

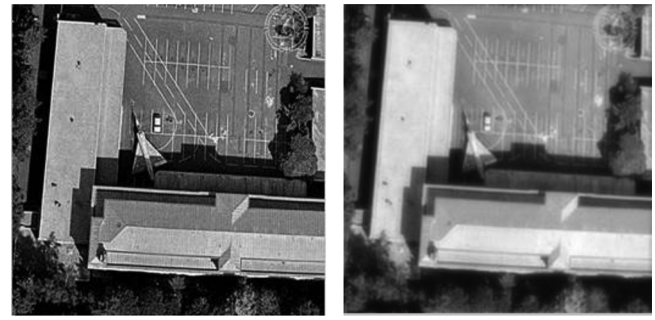

(a) (b)

Fig. 4. (a) Object image and (b) diffraction limited image.

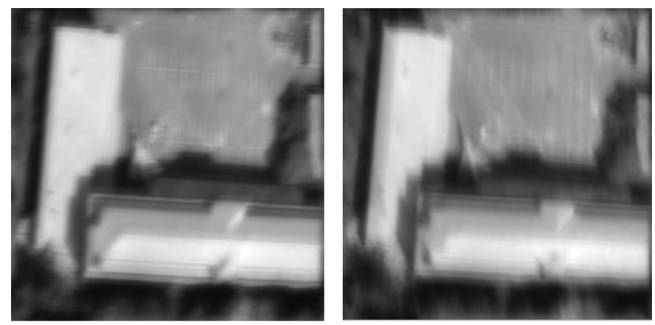

(a) (b)

Fig. 5. (a) Original focal image and (b) original defocused image.

Fig. 5 when all segmented sub-apertures have no other aberrations except co-phase errors:

Here, the SNR of the output images from CCD camera is set to 5 dB.

First, the global initial value of Zernike coefficients are confirmed by improved adaptive GA presented in this paper. The relevant parameters are set as below: the selected probability of the best individuals in non-linear rank-based selection $q = 0.236$, probability of adaptive arithmetic crossover is [0.95, 0.5], probability of adaptive non-uniform mutation is [0.8, 0.08], the size of population and evolution generations are set to 100 and 60 respectively.

The reconstructed wavefront aberration coefficients and residual errors are list in Table 2. The relationship between fitness value of cost function and evolution generations is shown in Fig. 6(a) and the residual phase distribution after initial alignment is given by Fig. 6(b).

3.2. Linearize OTF to obtain linear estimator of phase coefficients

According to the initial values in Section 3.1, after first alignment of segmented active optical analog system, co-phase errors of primary mirror are the residual errors in Table 2. Then the pair of focal and defocused degraded images with noise of the aligned system are given by Fig. 7, which are used for wavefront detection by linear correction algorithm based on PD under small phase aberrations.

The iterative linear correction algorithm based on PD can detect the wavefront aberrations effectively. However, the residual phase cannot always be small enough, thus OTF should be linearized at current estimator of Zernike coefficients in each iteration. During the alignment procedure, the aberrations are assumed to be the same in the considered time window. In time k, the estimator of aberration coefficients $\boldsymbol{\alpha}_k$ is $\hat{\boldsymbol{\alpha}}_k$, and then the residual aberration can be given by $\Delta\boldsymbol{\alpha}_k = \boldsymbol{\alpha}_k - \hat{\boldsymbol{\alpha}}_k$ which is used as initial aberration coefficients for the next iteration until reaching the set error tolerance.

Table 2
Initial reconstructed wavefront aberration coefficients and residual errors.

Index of sub-mirrors	Piston/λ			Tilt/λ			Tip/λ		
	p_{j0}	p_j	Δp_j	tx_{j0}	tx_j	Δtx_j	ty_{j0}	ty_j	Δty_j
1	0	0	0	0	0	0	0	0	0
2	−0.4	−0.4368	0.0368	0.25	0.3959	−0.1459	−0.3	−0.3907	0.0907
3	0	−0.1345	0.1345	−0.38	−0.3169	−0.0631	0.4	0.3268	0.0732
4	0.35	0.3818	−0.0318	0.4	0.2923	0.1077	−0.3	−0.2449	−0.0551
5	0.18	0.2019	−0.0219	0	0.0825	−0.0825	−0.26	−0.1477	−0.1123
6	0.3	0.1200	0.1800	0	0.0060	−0.0060	0	−0.0208	0.0208

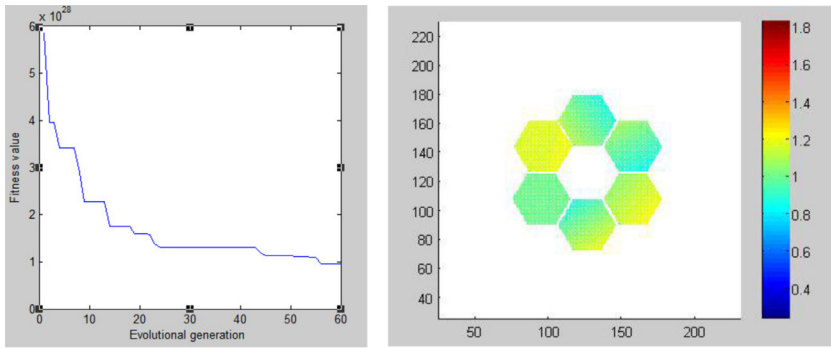

(a) (b)

Fig. 6. (a) The curve of fitness value varying with evolution generations and (b) residual phase distribution after initial alignment.

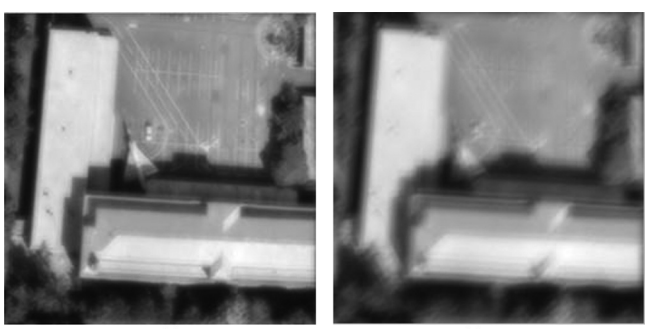

(a) (b)

Fig. 7. (a) Focal image after initial alignment and (b) defocused image after initial alignment.

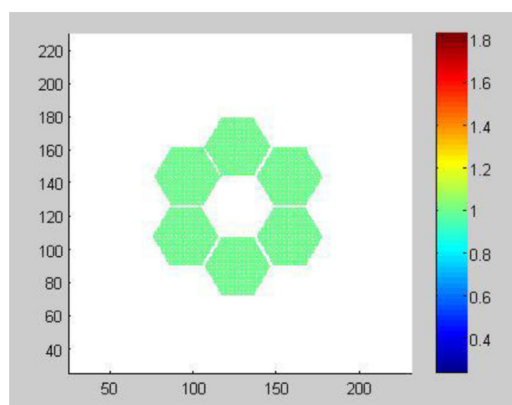

Fig. 8. Residual phase distribution after linear correction.

The recovered results are shown in Table 3:

After the aligning the optical analog system through linear correction algorithm, the final residual phase distribution is shown in Fig. 8:

According to Tables 1–3, the PV value of the simulated phase is 1.595λ, and its root-mean-square (RMS) is 0.256λ. After the initial alignment, the PV value and RMS of the phase are 0.3777λ and 0.0839λ respectively. The PV value and RMS of the finally reconstructed phase are $8.066 \times 10^{-5}\lambda$ and $1.4271 \times 10^{-5}\lambda$, which are quite small and totally acceptable.

The final recovered object is shown in Fig. 9 by using Eq. (7):

In order to verify the measurement accuracy of the proposed algorithm, another 100 sets of co-phase errors are generated randomly and applied to all sub-apertures under different CCD read-out noise. The residual errors of phase coefficients less than 0.01λ are considered effective reconstructions, then the ratio of effective recovery is shown as Table 4:

The results in Table 4 demonstrate the effectiveness of proposed algorithm. When the absolute value the wavefront aberration is less

Table 3
Final recovered wavefront aberrations coefficients and residual errors.

Index of sub-mirrors	Piston/λ			Tilt/λ			Tip/λ		
	p_{j0}	p_j	Δp_j	tx_{j0}	tx_j	Δtx_j	ty_{j0}	ty_j	Δty_j
1	0	0	0	0	0	0	0	0	0
2	0.0368	0.0367709	2.91e−5	−0.1495	−0.1495214	2.14e−5	0.0907	0.0907017	−1.7e−6
3	0.1345	0.1345015	−1.5e−6	−0.0631	−0.0630847	−1.53e−5	0.0732	0.0731904	9.6e−6
4	−0.0318	−0.0318020	2e−6	0.1077	0.1077256	2.56e−5	−0.0551	−0.0550723	−2.77e−5
5	−0.0219	−0.0218870	−1.3e−5	−0.0825	−0.0825003	3e−7	−0.1123	−0.1123001	1e−7
6	0.1800	0.1800011	−1.1e−6	−0.0060	−0.0060021	2.1e−6	0.0208	0.0208207	−2.07e−5

Fig. 9. Final reconstructed object image.

Table 4
Effective recovery ratio of 100 sets random co-phase errors.

CDD noise (dB)	Absolute value of co-phase error			
	<0.35λ	<0.4λ	<0.45λ	<0.5λ
0	99%	98%	96%	93%
5	98%	96%	95%	92%
10	96%	95%	93%	92%
20	95%	93%	91%	90%
30	92%	91%	89%	88%
40	90%	90%	87%	85%

than 0.4λ, the recovery efficiency is still very high even under heavy noise.

4. Conclusion

This paper presents a new hybrid algorithm to measure the co-phase errors and retrieve the object information. It utilizes an improved GA algorithm based on PD WFS to confirm the global initial value of aberration coefficients, and then linearizes the OTF to get the linear estimator of aberration coefficients under small residual phase by multi-iterations. The numerical experiments show that the proposed method is highly sensitive, noise tolerant and can fulfill the requirements for the phasing of segmented mirror telescopes. Future work will be concentrated on experimental verification of this co-phasing algorithm in laboratory.

Acknowledgment

This work was supported by National Natural Science Funds of China, Grant no. 61205143.

References

[1] P.A. Lightsey, C. Atkinson, M. Clampin, L.D. Feinberg, James Webb space telescope: large deployable cryogenic telescope in space, Opt. Eng. 51 (1) (2012) 011003-1–011003-19, http://dx.doi.org/10.1117/1.OE.51.1.011003.
[2] V.G. Orlov, S. Cuevas, F. Garfias, et al., Co-phasing of segmented mirror telescopes with curvature sensing, in: Astronomical Telescopes and Instrumentation, International Society for Optics and Photonics, 2000, pp. 540–551.
[3] G. Chanan, M. Troy, F. Dekens, et al., Phasing the mirror segments of the Keck telescopes: the broadband phasing algorithm, Appl. Opt. 37 (1) (1998) 140–155.
[4] G.C. Dente, M.L. Tilton, Segmented mirror phasing using the focal-plane intensity, Appl. Opt. 51 (3) (2012) 295–301.
[5] D. Qu, Y. Zhao, L. Dong, et al., New method for detecting the piston of segmented mirrors: a modification of the peak ratio technique, in: International Symposium on Photoelectronic Detection and Imaging: Technology and Applications 2007, International Society for Optics and Photonics, 2007, 66240N-66240N-9.
[6] P.G. Tuthill, J.D. Monnier, W.C. Danchi, et al., Michelson interferometry with the Keck I telescope, Publ. Astron. Soc. Pac. 112 (770) (2000) 555–565.
[7] H. Yang, Y. Li, Generalized phase diversity wavefront sensing based on stochastic parallel optimization algorithm, Procedia Eng. 24 (2011) 43–47.
[8] R.G. Paxman, J.R. Fienup, Optical misalignment sensing and image reconstruction using phase diversity, JOSA A 5 (6) (1988) 914–923.
[9] S. Meimon, E. Delavaquerie, F. Cassaing, et al., Phasing segmented telescopes with long-exposure phase diversity images, in: SPIE Astronomical Telescopes + Instrumentation, International Society for Optics and Photonics, 2008, 701214-701214-10.
[10] C. Li, S. Zhang, Co-phasing of the segmented mirror based on the generalized phase diversity wavefront sensor, in: SPIE Astronomical Telescopes + Instrumentation, International Society for Optics and Photonics, 2012, 84500B-84500B-6.
[11] J.H. Holland, Genetic algorithms and the optimal allocation of trials, SIAM J. Comput. 2 (2) (1973) 88–105.
[12] H. Yang, Y. Li, Genetic algorithm for phase retrieval of generalized phase diversity, Energy Procedia 13 (2011) 4806–4811.
[13] L. Shitong, Y. Jianfeng, X. Bin, A new phase diversity wave-front error sensing method based on genetic algorithm, Acta Opt. Sin. 30 (4) (2010) 1015–1019.
[14] J.E. Nelson, T.S. Mast, S.M. Faber, The design of the Keck observatory and telescope, Keck Obs. Rep. 90 (1985).
[15] Z. Liu, S.Q. Wang, C.H. Rao, Comparative metrics for far-field intensity and piston error in sparse optical synthetic aperture telescope system, Optik 124 (17) (2013) 2979–2984.
[16] L.M. Mugnier, A. Blanc, J. Idier, Phase diversity: a technique for wave-front sensing and for diffraction-limited imaging, Adv. Imaging Electron Phys. 141 (2006) 3–77.
[17] C.S. Smith, R. Marinică, A.J. Den Dekker, et al., Iterative linear focal-plane wavefront correction, JOSA A 30 (10) (2013) 2002–2011.